JOURNAL OF GEOPHYSICAL RESEARCH: OCEANS, VOL. 118, 3752–3763, doi:10.1002/jgrc.20264, 2013

Detection of linear trends in multisensor time series in the presence of autocorrelated noise: Application to the chlorophyll-a SeaWiFS and MERIS data sets and extrapolation to the incoming Sentinel 3-OLCI mission

Bertrand Saulquin,[1,2] Ronan Fablet,[2,3] Antoine Mangin,[1] Grégoire Mercier,[2,3] David Antoine,[4,5] and Odile Fanton d'Andon[1]

Received 31 January 2013; revised 24 April 2013; accepted 31 May 2013; published 1 August 2013.

[1] The detection of long-term trends in geophysical time series is a key issue in climate change studies. This detection is affected by many factors: the size of the trend to be detected, the length of the available data sets, and the noise properties. Although the noise autocorrelation observed in geophysical time series does not bias the trend estimate, it affects the estimation of its uncertainty and consequently the ability to detect, or not, a significant trend. Ignoring the noise autocorrelation level typically leads to an overdetection of significant trends. Due to satellite lifetime, usually between 5 and 10 years, sea surface time series do not cover the same period and are acquired by different sensors with different characteristics. These differences lead to unknown level shifts (biases) between the data sets, which affect the trend detection. In this work, we develop a generic framework to detect and evaluate linear trends and level shifts in multisensor time series of satellite chlorophyll-a concentrations, as provided by the Medium Resolution Imaging Spectrometer instrument (MERIS) and sea-viewing wide field-of-view sensor (SeaWiFS) ocean-color missions. We also discuss the optimization of the observation networks, in terms of needed time overlap between successive time series to reduce the uncertainty on the detection of long-term trends. For the incoming Sentinel 3-Ocean and Land Color Instrument (3-OLCI) mission that should be launched at the end of 2014, we propose a global map of the number of months of observations to enhance the trend detection performed with the joint SeaWiFS-MERIS analysis.

Citation: Saulquin, B., R. Fablet, A. Mangin, G. Mercier, D. Antoine, and O. Fanton d'Andon (2013), Detection of linear trends in multisensor time series in the presence of autocorrelated noise: Application to the chlorophyll-a SeaWiFS and MERIS data sets and extrapolation to the incoming Sentinel 3-OLCI mission, *J. Geophys. Res. Oceans*, *118*, 3752–3763, doi:10.1002/jgrc.20264.

1. Introduction

[2] A variety of studies have addressed the detection of long-term trends in autocorrelated processes. *Tiao et al*. [1990] showed that the trend estimation uncertainty is strongly affected by the variability and the autocorrelation of the underlying noise process. Environmental data typically involve strong autocorrelation level [*Frankignoul and Hasselmann*, 1977]. For instance, a positive anomaly in the observed wind or temperature on a given day is often associated with similar conditions the following days. This natural autocorrelation is the result of local conditions but also of large-scale signals such as, for instance, the well-known El-Niño-La-Niña oscillation [*Philander*, 1990; *Torrence and Webster*, 1998]. It also implies that the day-to-day or month-to-month observations are no more independent one from each other, and that the "real" number of independent observations available to detect a trend is significantly lower than in uncorrelated cases [*Clifford et al*., 1989; *Tiao et al*., 1990; *Dutilleul*, 1993].

[3] Since the end of the 1970s, satellite ocean-color observations have been providing large-scale measurements of the water-leaving radiance [*McClain*, 2009], i.e., the light intensity estimated at the surface of the ocean at different wavelengths in the visible from 400 to 700 nm and near infrared. These radiances are used as inputs of

[1]ACRI-ST, Sophia-Antipolis, Sophia-Antipolis, France.
[2]Institut Mines-Telecom, Télécom Bretagne, UMR CNRS 3192 Lab-STICC Brest, France.
[3]Université Européenne de Bretagne, Rennes, France.
[4]Laboratoire d'Océanographie de Villefranche, Centre National de la Recherche Scientifique (CNRS) and Université Pierre et Marie Curie, Paris 06, Villefranche-sur-Mer, France.
[5]Now at Department of Imaging and Applied Physics, Remote Sensing and Satellite Research Group, Curtin University, Perth, Australia.

Corresponding author: B. Saulquin, ACRI-ST, Sophia-Antipolis, 260 Rt. du Pin Montard, BP 234, FR-06904 Sophia-Antipolis CEDEX, France. (bertrand.saulquin@acri-st.fr)

2169-9275/13/10.1002/jgrc.20264

Table 1. List of Symbols[a]

Symbol	Designation	Unit
y_t	2-D time series	mg m^{-3}
μ	Intercept	mg m^{-3}
ω	Linear trend	mg m^{-3} yr^{-1}
σ_ω	Uncertainty of trend	mg m^{-3} yr^{-1}
S_t	Seasonal component	n.a.
N_t	Autocorrelated (red) noise	n.a.
σ_N^2	Red noise variance	mg^2 m^{-6} yr^{-2}
ε_t	White noise	n.a.
σ^2	White noise variance	mg^2 m^{-6} yr^{-2}
ϕ	Noise autocorrelation	No unit
δ	Level shift	mg m^{-3}
$\lvert\omega\rvert/\sigma_\omega$	Trend detection variable	No unit
α	Correlation between Y_{1t} and Y_{2t}	No unit
N	Length of the time series	Months
T_0	Start time of the second time series	Months

[a]Units are relative to the studied parameter, here the chl-a.

inversion algorithms to retrieve biogeochemical parameters. Among available ocean-color variables, the most popular is the chlorophyll-a (chl-a) concentration [*Maritorena et al*., 2010; *O'Reilly et al*., 1998; *Morel et al*., 2006], which is used in this work. The limited lifetime of space-based sensors implies that the long-term variability of such geophysical parameter can only be evaluated using a combination of time series. Among the historical ocean-color sensors, the most widely used are the NASA sea-viewing wide field-of-view sensor (SeaWiFS) [*Hooker et al*., 1992] that operated from September 1997 to December 2010, the European Spatial Agency (ESA) Medium Resolution Imaging Spectrometer Instrument (MERIS) [*Rast et al*., 1999], in activity from April 2002 to April 2012, and the NASA Moderate Resolution Imaging Spectroradiometer, MODIS-AQUA [*Salomonson et al*., 1992], launched in July 2002 which is still operational. Ocean-color data with limited wavelength range are also available from the Coastal Zone Color Scanner (CZCS), which operated from 1978 to 1986 [*Evans and Gordon*, 1994].

[4] Trend estimation using the single SeaWiFS data set has been previously addressed using different methods. *Gregg et al*. [2005] estimated trends in the chl-a over the period 1998–2003 using a classical linear trend estimation. Recently, *Vantrepotte and Mélin* [2009] used the census X11 method (adapted from *Pezzulli et al*. [2005]), and *Henson et al*. [2010] used a simple model based on a three-component decomposition according to a seasonal signal, a linear trend, and an autocorrelated noise, to estimate trends over the period 1998–2007. Trend estimation from multisensor data sets has been impaired until now because of intercalibration uncertainties among available data sets. For instance, *Antoine et al*. [2005] reanalyzed the CZCS and SeaWiFS time series to study the chl-a changes between these two missions, but they could not attribute to the changes they observed to a long-term trend.

[5] This paper goes beyond intercalibration issues and deals with the detectability of a linear trend or its significance from multisensor data sets. From a methodological point of view, we extend the statistical analysis of linear trends in single-sensor time series in the presence of autocorrelated noise [*Tiao et al*., 1990; *Weatherhead et al*., 1998; *Henson et al*., 2010] to multisensor time series. In particular, we address both time overlaps and time gaps between time series. We report and discuss an application to the MERIS and the SeaWiFS chl-a data sets, which clearly demonstrate the gain of a multisensor analysis. We propose here a simple oceanographic description of the observed trends assuming that the full understanding of the long-term trends in the chl-a should be studied in conjunction with the temperature and the sea surface level.

[6] Besides, we investigate how the time overlap between successive satellite missions could be optimized to improve the detectability of long-term trends. The Global Monitoring for Environment and Security (GMES) Sentinel 3 (S3) mission should be launched at the end of 2014. This mission will carry the Ocean and Land Color Instrument (OLCI), an imaging spectrometer that will deliver multi-channel wide-swath optical measurements of ocean and land surfaces, providing a new time series of chl-a observed from space. We also exploit the proposed statistical methodology to evaluate the duration of the S3-OLCI observation series required to improve the joint SeaWiFS-MERIS trend detection based on the hypothesis that the OLCI-MERIS level shift uncertainty will be of the same magnitude as the SeaWiFS-MERIS one.

2. Trend Estimation

[7] In Table 1 is listed the used symbols with their description.

2.1. Statistical Modeling

2.1.1. Single-Sensor Data Set

[8] The observed geophysical time series, y_t, are modeled as a sum of three components: a long-term linear trend, a seasonal pattern, and a noise process, as follows:

$$y_t = \mu + \omega t + S_t + N_t, \qquad t = 1 \ldots n, \tag{1}$$

where n is the length of the time series, μ is the intercept term, ω is the linear trend, and S_t is the seasonal component which includes annual and semiannual terms. We chose here a similar representation of S_t as in *Weatherhead et al*. [1998]:

$$S_t = \sum_{i=1}^{4} a_i \cos\left(\frac{2\pi i t}{12}\right) + b_i \sin\left(\frac{2\pi i t}{12}\right) \tag{2}$$

[9] Here S_t is identical from year to year with a null sum over a year (S_t does not contribute to a global trend). N_t is the correlated noise (red noise), assumed to be a first-order autoregressive process, AR(1):

$$N_t = \phi N_{t-1} + \epsilon_t \tag{3}$$

where ε_t is a white noise, i.e., an independent random variable with zero mean and variance σ^2. The stationary condition for N_t imposes that $-1 < \phi < 1$. In the presence of autocorrelation, the residuals are no longer independent, and the calibration of model (1) involves a generalized least square (GLS) estimator [*Aitken*, 1935; *Davidson and MacKinnon*, 1993]. The latter relies on the estimation of

the covariance matrix γ of the residuals N_t, generally unknown. For $\phi = 0$, γ is diagonal with term value equal to the variance of the white noise. If $\phi \cong 0$, the diagonal terms are still equal to the variance of the red noise, and the other terms are estimated as lagged covariance between noise realizations:

$$\mathrm{cov}\,(N_t, N_{t+h}) = \frac{\phi^n}{1-\phi^2} \tag{4}$$

[10] In practice, the estimation of the model parameters in equation (1) may be achieved using several methods. Among them Prais-Winsten [*Prais and Winsten*, 1954] and *Cochrane and Orcutt* [1949] methods aim at transforming (equation (1)) into an expression involving an uncorrelated noise residual [*Tiao et al.*, 1990; *Weatherhead et al.*, 1998]:

$$y_t^* = \mu + \omega t^* + S_{t^*} + \epsilon_t \tag{5}$$

[11] Given equation (5), the standard ordinary least squares (OLS) [*Aitken*, 1935; *Russel*, 1993] estimator may be used. The trend estimation is not affected by the noise autocorrelation but its uncertainty strongly depends on ϕ:

$$\sigma_\omega = \frac{\sigma}{(1-\phi)\sqrt{\sum_{i=1}^{n}(t-\bar{t})^2}} \tag{6}$$

[12] The parameter σ_ω can be expressed as a function of the white noise variance, $\sigma^2 = \sigma_N{}^2(1-\phi^2)$, and the trend coefficient uncertainty, G, defined as the uncertainty on the trend estimate normalized with respect to the white noise variance:

$$\sigma_\omega = \sigma G(n, \phi) \tag{7}$$

2.1.2. Multisensor Data Set

[13] In this work we investigate a generalization to data sets acquired by different sensors for possibly different time periods. While the increase of the number of observations may decrease the variance of the trend estimation compared to the single-sensor case, the presence of unknown level shifts between the time series may significantly affect the uncertainty of the trend estimation. For the sake of simplicity, we consider in the following a two-sensor data set, but the proposed framework generalizes to three or more sensors. Given a two-sensor data set, we assume that the two time series share the same long-term trend and seasonal patterns but involve an unknown level shift and correlated noise processes:

$$y_t = \mu + \omega t + S_t + N_{1t}, \qquad t = 1 \ldots n_1 \tag{8a}$$

$$y_t = \mu + \omega t + \delta U + S_t + N_{2t}, \qquad t = T_0 \ldots n_2 \tag{8b}$$

where time t is in any case relative to the start of the first time series, which is considered as the reference. T_0 is the starting time of the second time series, and n_1 and n_2 are the length of the first and second time series, respectively. The parameters μ and ω are the intercept term and the linear trend shared by the two time series, respectively. The parameter δ is the unknown level shift of the second time series compared to the first one, supposed here as constant in time. $U = 1$ for $t \geq T_0$ and $U = 0$ for $t < T_0$. N_{1t} and N_{2t} are the autocorrelated noises of the two time series.

[14] The estimation of the level shift between the two time series using an intercalibration procedure [*Johnson et al.*, 1996] prior to the estimation of the shared linear trend is statistically relevant if one accounts for the uncertainty of the level shift in the variance of the trend estimate. Neglecting this uncertainty resorts to a null-shift case. This is equivalent to considering a single time series and would greatly underestimate the variance of the trend estimate. To fit model parameters in equation (8), we consider an iterative procedure adapted from the *Cochrane and Orcutt* [1949] transformation. Details on the numerical resolution of equation (8) are given in Appendix A. Only the estimates obtained after convergence that satisfy the 95% detection threshold are considered in our analysis. This procedure leads to the estimation of the model parameters u, ω, S, δ as well as the variance of these estimates, and the variance of the uncorrelated residuals σ^2.

2.2. Detecting Significant Trends

[15] The detectability of a trend or its significance may be treated from different but coincident points of views. It generally relies on the estimation of the standard deviation of the trend estimate (or the associated interval of confidence), and less usually on the number of observations required to detect a trend among a noise with a given variance. Formally, the statistical assessment of the significance of a trend in a time series of length n resorts to testing either the variable $|\hat{\omega}|/\sigma_{\hat{\omega}}$ or the variable $\frac{\hat{r}\sqrt{n-2}}{\sqrt{1-\hat{r}^2}}$, with r being the coefficient of correlation between the time series and the trend. Both tests are similar [*Scherrer*, 1984] and both variables theoretically follow a Student's T distribution with $n-2$ degrees of freedom [*Haan*, 1977; *Legendre and Legendre*, 1998; *Scherrer*, 1984]. Under the considered red noise model assumption, the 90% confidence level is reached for $|\hat{\omega}|/\sigma_{\hat{\omega}} > 1.64$ and the 95% confidence level for $|\hat{\omega}|/\sigma_{\hat{\omega}} > 1.96$. In the subsequent, we consider a 95% confidence level, such that we test for $|\hat{\omega}|/\sigma_{\hat{\omega}} > 1.96$.

3. Application to the Two-Sensor SeaWiFS-MERIS Data Set

3.1. Data Set

[16] *Tiao et al.* [1990] showed that the existence of a moderate positive value of Φ in the daily measurements is enough to make the trend estimate insensitive to changes in the temporal sampling. Compared to the daily data, the monthly averaged data will lower the length of the time series and the autocorrelation leading to similar trend detection. It implies that geophysical data sets, associated with high autocorrelation levels, may be analyzed using the monthly time series. Two data sets are used here, the global 1998–2010 SeaWiFS monthly chl-a products estimated using the Ocean Chlorophyll 4-band algorithm (OC4) [*O'Reilly et al.*, 1998, 2000], and the global 2003–2011 MERIS chl-a monthly estimated using the MERIS OC4

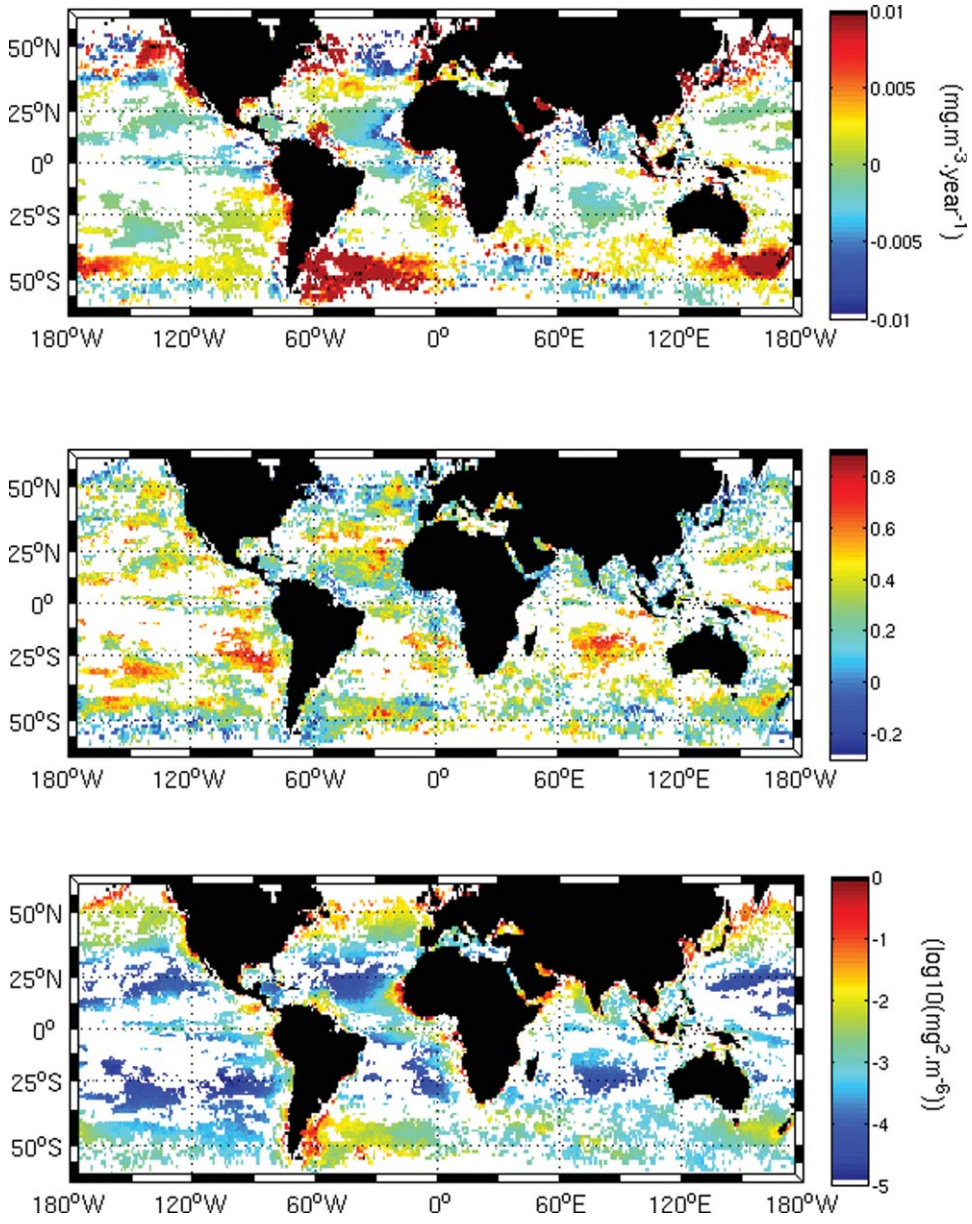

Figure 1. Estimated parameters for the single-sensor model (equation (1)) using the SeaWiFS monthly data (1998–2010). (a) Significant linear trends, $\hat{\omega}$, with respect to a 95% confidence level, (b) noise autocorrelation $\hat{\phi}$, and (c) noise variance $\hat{\sigma}^2$.

algorithm [*Morel et al.*, 2007]. Data were projected onto a regular $1^\circ \times 1^\circ$ grid, and time series with more than 30% of missing data were withdrawn from the analysis, leaving 31,829 for both data sets. For each location of the $1^\circ \times 1^\circ$ grid, a climatology estimated from the available observations has been subtracted to the original time series to remove the seasonal signal, S_t. Neither spatial nor temporal interpolations were performed on the data set. The value of T_0 used in equation (8), i.e., the starting time of the MERIS time series, is equal to 60 months.

3.2. Single-Sensor Linear Trend Detection Using the SeaWiFS Data Set

[17] Figure 1 shows for the period 1998–2010 the estimated model parameters for the single-sensor model (equation (1)) using the SeaWiFS monthly chl-a data set, namely, the long-term trend $\hat{\omega}$, the noise autocorrelation $\hat{\phi}$, and the white noise variance $\hat{\sigma}^2$. Overall, we detect significant linear trends for 41% of the 31,829 time series (Figure 1). There are several coherent patches with significant trends. The typical magnitude of trends in the chl-a is approximately ± 0.003 mg m^{-3} yr^{-1}, with positive peak values of $+0.009$ mg m^{-3} yr^{-1} at the eastern part of the Argentina, the south of Australia, the Behring Sea, and specific coastal areas. Negative peak values of -0.009 mg m^{-3} yr^{-1} are reached in the North Atlantic and the Arabian Sea. We observe in the intertropical region a majority of negative trends in the chl-a concentration with a mean value of -0.002 mg m^{-3} yr^{-1}.

[18] Compared to previous trend estimations performed on the SeaWiFS data set, *Gregg and Casey* [2004] observed globally comparable trends on the period 1998–

2003 with the exception of the eastern part of Africa that do not show anymore a positive trend. This difference may be explained either by the absence of a global linear trend for the entire 1998–2010 period or by the ignorance of noise autocorrelation by *Gregg and Casey* [2004] and *Gregg et al.* [2005]. *Henson et al*. [2010] showed a similar global distribution of the trend estimates for this period using the same single-sensor model (equation (1)) and the 1998–2007 SeaWiFS data set, with nevertheless less positive trends east of South Argentina. This suggests that the data from 2008 to 2010 contributed significantly to the detection of significant positive trends of chl-a in this area.

[19] Concerning the noise autocorrelation $\hat{\phi}$, the mean observed value over the globe is 0.3 (Figure 1b). Minimum values of -0.2 are observed locally in the southern part and specific coastal areas. Maximum $\hat{\phi}$ values of 0.75 are observed at 30°S in the Indian Ocean and the East Chile. Globally, the noise autocorrelation is greater in the tropical region with a mean value of 0.35 between 30°S and 30°N, compared to a mean value of 0.25 for latitudes south of 60°S or north of 60°N.

[20] The estimated variance of the residuals (Figure 1c) shows latitudinal and coastward distribution with greater values observed at high latitudes and along the shores and appears correlated to the mean values of the chl-a distribution [*Blunden et al.,* 2011]. In the intertropical zone, y_t variance is lower than the one observed at high latitudes, and the variability is led by nonseasonal signals leading to a large correlation in the residuals (large values of $\hat{\phi}$).

3.3. Single-Sensor Linear Trend Detection Using the MERIS Data Set

[21] We also report the same analysis as above for the 2003–2011 MERIS data set (Figure 2). Although the MERIS data set is only a 10 year time series compared to the 13 years of data available for the SeaWiFS data set, we detect significant linear trends for 50% of the 2003–2011 MERIS time series (41% for the SeaWiFS data, respectively). The Equatorial Pacific shows a linear decrease of -0.002 mg m^{-3} yr^{-1} surrounded by a large belt of positive trends, with a mean value of 0.006 mg m^{-3} yr^{-1}, starting from the East Papua New Guinea and ending in the north in the Mexico and in the south in the north of Chile leading to a wishbone shape of positive trends in the Equatorial Pacific. This region is well known to be strongly influenced by the El Niño–Southern Oscillation (ENSO) signal (http://www.srh.weather.gov/srh/jetstream/tropics/enso.htm). In this region, the difference in terms of detection between SeaWiFS and MERIS data set is clearly visible. A major ENSO–Niño event occurred during the 1997–1998 followed by a ENSO–Niña period during 1998–2000. Phytoplankton productivity relies on the availability of sunlight, macronutrients (e.g., nitrogen and phosphorous), and micronutrients (e.g., iron) and thus is sensitive to climate-driven changes in the delivery of these resources to the euphotic zone. *Turk et al*. [2011] showed that the ENSO oscillation strongly impact the chl-a and the primary production in the Equatorial Pacific, and one can clearly see Figure 1a that using the SeaWiFS 1998–2010 data set a limited number of significant trends are detected in this area compared to the MERIS data set over the period 2003–2011: nonstationary processes such as El-Niño-La-Niña tend to reduce the ability to detect a trend. The problem of estimating and removing ENSO-related variations from climate records has been addressed in many previous studies for the sea surface temperature (SST) using a variety of methods. In this spirit, *Compo and Sardeshmukh* [2010] used the ENSO pattern filter (EPF) [*Alexander et al*., 2008], developed to remove the contribution of ENSO patterns in the SST from 1871 to 2006. Satellite-derived ocean-color time series are nevertheless shorter and show a greater intraseasonal variability. This alters the ability of filtering the long-term variability caused by such signals. This type of filtering has not yet been implemented for the chl-a time series, and its evaluation is in any case beyond the scope of this paper, as we do not discuss of the quality of the input data.

[22] The estimated noise autocorrelation shows a similar geographical distribution as observed for the SeaWiFS data set with nevertheless a large band of high autocorrelated noise in the South Pacific. The residual variance is distributed similarly to the one estimated using SeaWiFS with nevertheless a northward extension of the detected trends.

3.4. Two-Sensor Linear Trend Detection Using Both MERIS and SeaWiFS Data

[23] Using the two-sensor model (equation (8)), the joint analysis (Figure 3) of the MERIS and SeaWiFS time series leads to 60% of significant detections of linear trends for the period 1998–2011 (50% and 41% for MERIS and SeaWiFS data alone, respectively). It resorts to much clearer patterns at a global scale for the period 1998–2011 compared to the period 1998–2010 and 2003–2011 considered individually. In Table 2 we summarize at ocean-scale trend estimated statistics. At global scale, the observed median value in the significant trends is 2.83×10^{-4} mg m^{-3} yr^{-1}. This value is low and opposite to the estimated trend by *Boyce et al*. [2010] for the twentieth century using this time in situ data. Indian Ocean shows the largest median value with a decreasing value of -1.40×10^{-3} mg m^{-3} yr^{-1}, while the Pacific and the Atlantic show similar median positive trends of 7.27×10^{-4} and 8.27×10^{-4} mg m^{-3} yr^{-1}, respectively. Regarding coastal areas, we detect positive trends especially in the Bering Sea, the Pacific shores of the United States, and the Patagonian Shelf (Figure 3a). Regarding the open ocean, southern regions show as observed in Figures 1a and 2a, a majority of positive trends with local maximum at $+0.009$ mg m^{-3} yr^{-1} in the eastern part of South Argentina and the southeastern part of Australia. Although we do not discuss here of the quality of the data set, we underline nevertheless that both algorithms, SeaWiFS OC4 and MERIS OC4, are calibrated for open ocean waters where the observed radiance is constrained by the water and the chl-a absorption properties. In coastal areas and specific areas, the effect of the suspended matters and the colored dissolved organic matters may alter the observed radiances leading to positive biases in the estimated chl-a retrieval using the OC4 algorithms and possibly affecting the trend estimation in such areas. A full discussion on the estimation of optical properties in coastal areas is available in *International Ocean-Color Coordinating Group* [2000].

[24] The "wishbone" pattern in the Equatorial Pacific clearly appears in Figure 3b with this time some extensions

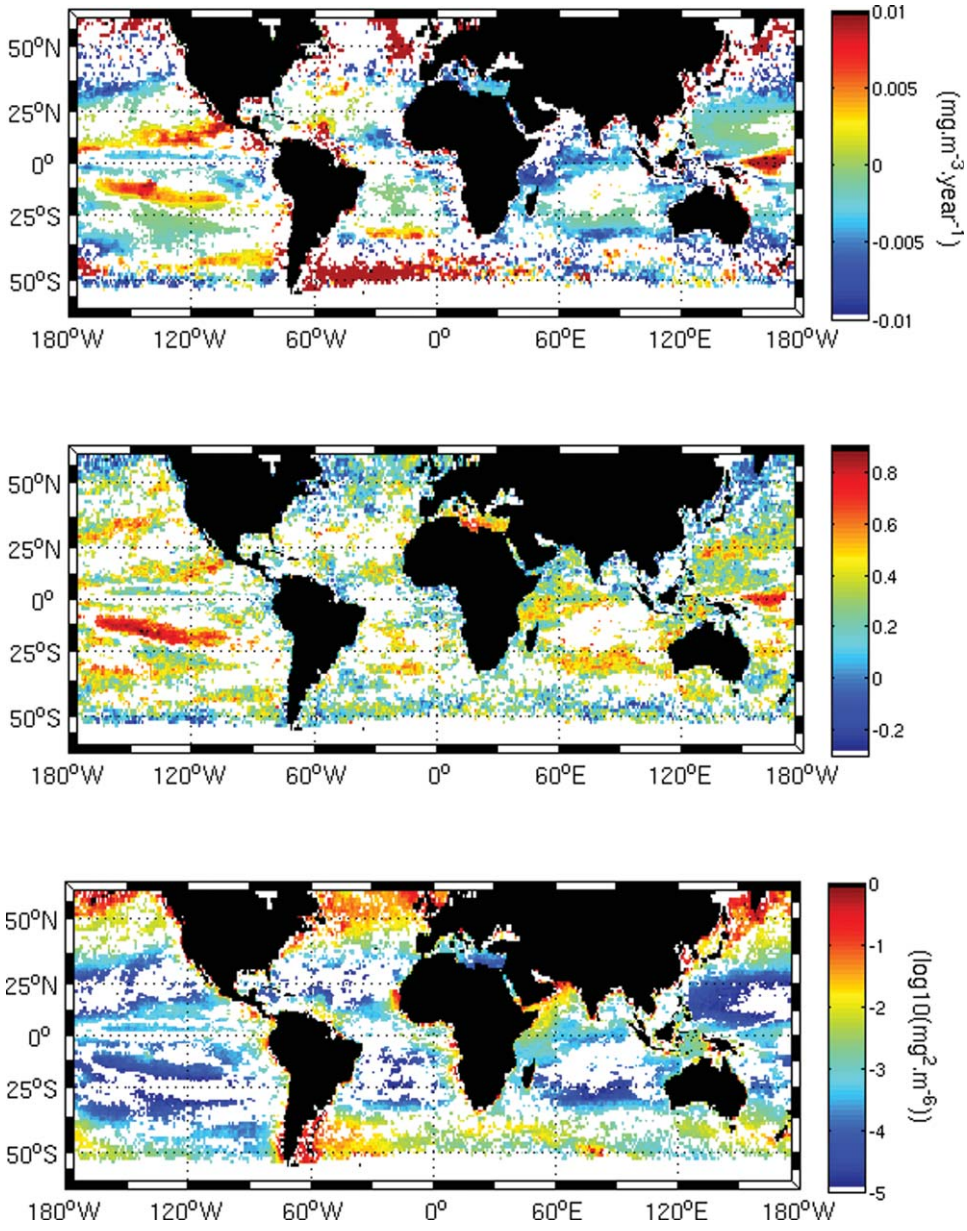

Figure 2. Estimated parameters for the single-sensor model (equation (1)) using the MERIS data set (2003–2011). (a) Significant linear trends, $\hat{\omega}$, with respect to a 95% confidence level, (b) noise autocorrelation $\hat{\phi}$, and (c) noise variance $\hat{\sigma}^2$.

of the positive trends from the Florida to the Mediterranean Sea and from Brazil to South Africa. This Atlantic extension of this structure was not visible using the SeaWiFS (Figure 3a) data set and only partially visible using the MERIS data set.

[25] Some coastal regions depict negative trends with a minimum of -0.009 mg m^{-3} yr^{-1} in the equatorial area, the North Atlantic, and the North Pacific. From the joint analysis, the Indian gyre and more generally the Indian Ocean show a global negative trend except for its southern area. The decline in the global gyres in the productivity, directly linked to the chl-a, was also observed by *Polovina et al*. [2008].

[26] In the Atlantic, the intertropical zone shows a low decrease of -0.002 mg m^{-3} yr^{-1}. In the South Atlantic and below 40°S, the trend increases positively. Regarding the North Atlantic, we detect an increase of the chl-a in the North Atlantic Current and the Gulf Stream, and northward, the Atlantic Western part shows a positive trend conversely to the eastern part.

[27] The estimated shift between the two chl-a data sets is reported Figure 3b. Its magnitude, conversely to its uncertainty, does not affect the trend estimation. Maximum positive shift values are observed in the North Atlantic with local values of 0.08 mg m^{-3} yr^{-1} of positive shift for the MERIS OC4 compared to the SeaWiFS OC4 chl-a. Conversely, negative maximum values are observed in the Tasman Sea. The large shift values observed at high latitudes might be related to local differences in the atmospheric corrections used for each sensor [*International Ocean-Color Coordinating Group*, 2010].

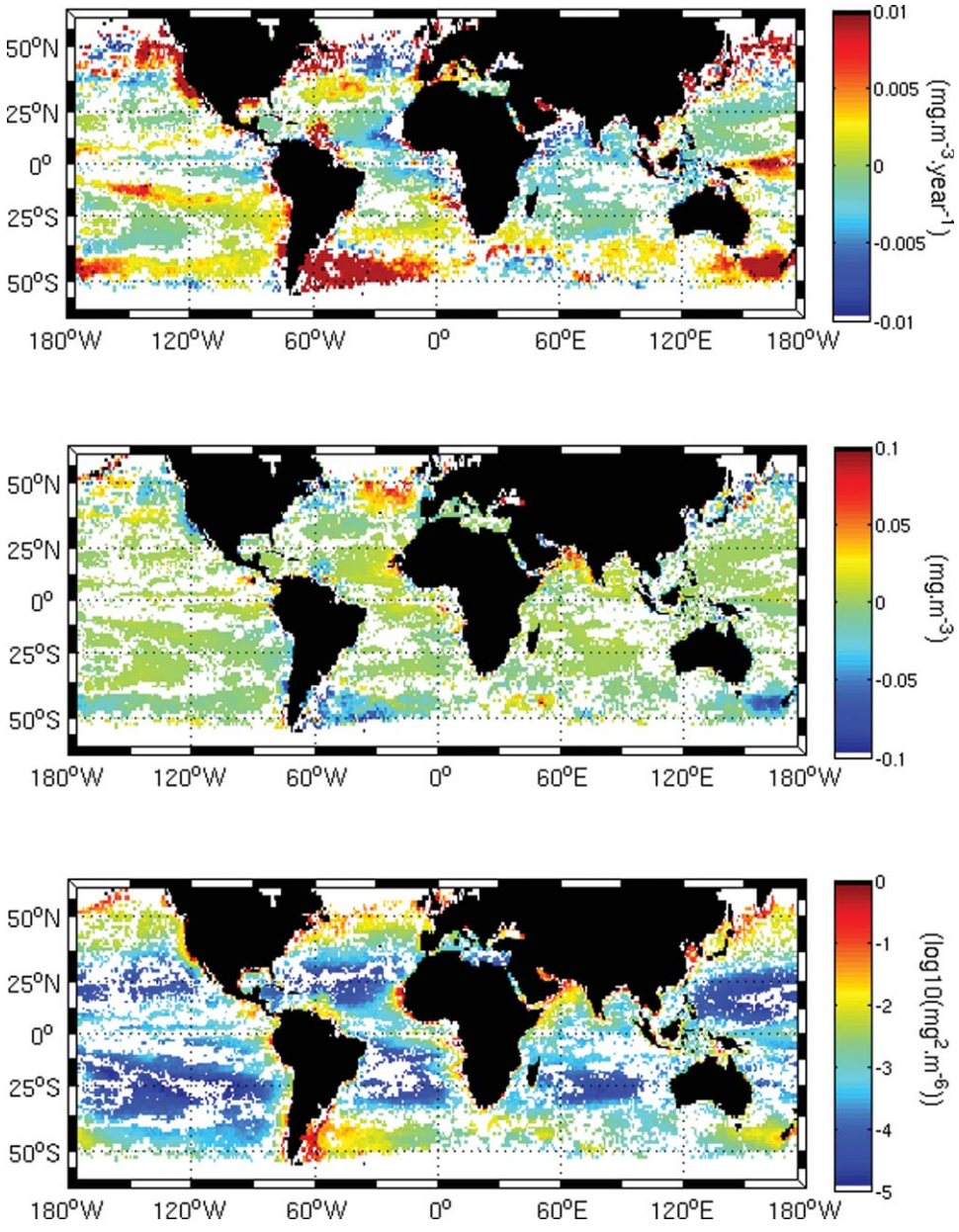

Figure 3. Estimated parameters for the multisensor model (equation (8)) using the SeaWiFS and the MERIS data set (1998–2011). (a) Significant linear trends, $\hat{\omega}$, with respect to a 95% confidence level, (b) level shift $\hat{\delta}$, and (c) noise variance $\hat{\sigma}^2$.

[28] The estimated variance of the residuals (Figure 3c) shows greater values for the high latitudes and on the shores directly correlated to the mean values of the chl-a distribution [*Blunden et al.*, 2011] as observed Figures 1c and 2c.

4. Optimization of a Time Overlap Between Successive Missions for Long-Term Monitoring and Impact of the Incoming ESA Sentinel 3-OLCI Mission

[29] The proposed multisensor model (equation (8)) provides the basis for investigating the extent to which the time overlap between successive missions may be optimized to reduce the uncertainty on the long-term detection of linear trends in geophysical time series.

[30] From equation (7), the uncertainty of the trend estimation (equation (8)) can be expressed as a function of model parameters (Appendix A):

Table 2. Statistics at Large Scale on the Estimated Significant Trends in the Chl-a (mg m^{-3} yr^{-1}) Over the Period 1998–2011

	Median($\hat{\omega}$)	Min($\hat{\omega}$)	Max($\hat{\omega}$)	$\sigma\hat{\omega}$
Global	2.83×10^{-4}	1.59×10^{-1}	1.0×10^{-2}	3.20×10^{-3}
Atlantic	8.27×10^{-4}	-1.59×10^{-1}	1.0×10^{-2}	4.60×10^{-3}
Pacific	7.27×10^{-4}	-7.49×10^{-2}	1.0×10^{-2}	2.80×10^{-3}
Indian Ocean	-1.40×10^{-3}	-1.14×10^{-1}	9.60×10^{-3}	2.00×10^{-3}

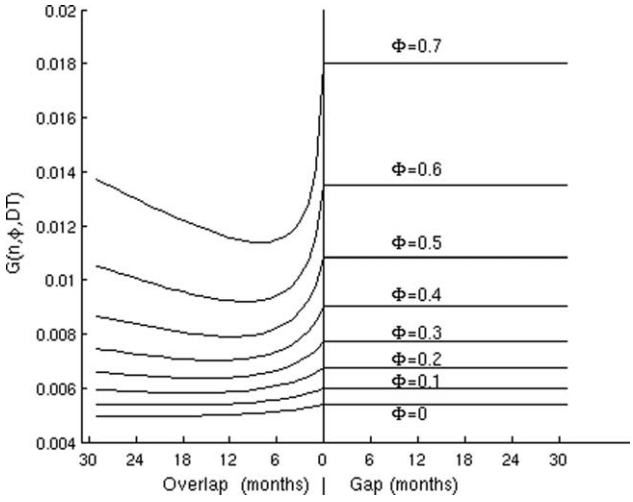

Figure 4. Effect of the time overlap or the gap time (in months) between two time series of 60 months on the trend uncertainty coefficient G (equation (9)).

$$\sigma_\omega = \sigma G(n, \phi, \mathrm{DT}, \alpha) \tag{9}$$

where G is the trend uncertainty which in case of the use of two time series is a function of n, ϕ, DT, n the total number of nonredundant months between two time series, and ϕ the observed autocorrelation (we supposed here $\phi_1 = \phi_2 = \phi$). DT is the starting time of the second time series, given the first time series is assumed to start at time $t = 0$. Depending on parameter DT, we cover both time overlap between the two series (DT$< n_1$, the length of the first time series) as well as time gaps (DT$> n_1$). The parameter α is the correlation coefficient between the two white noise processes and σ^2 the weighted variance expressed as a function of the two white noise variances (cf. Appendix B).

[31] Given two time series of 60 months, we report the uncertainty coefficient G for the trend estimate as a function of parameters ϕ, n, and DT (Figures 4 and 5). Parameter α was set to 0.7, the mean correlation value observed between MERIS and SeaWiFS. The uncertainty coefficient G (and consequently σ_w) increases with ϕ (Figure 4). When an overlap is present (DT < 60 months), G decreases with the time overlap until it reaches a minimum value that depends on the autocorrelation value. This minimum corresponds to the optimal value of the time overlap between two time series to optimize the balance between the uncertainty on the shift parameter δ and the length of the two time series. For $\phi = 0.3$, i.e., the mean value observed for SeaWiFS (Figure 1b), the minimum is reached for 12 months of time overlap. When no overlap is present and the time gap increases, the uncertainty on the trend remains constant as the estimation of the trend resorts to analyzing independent time series only sharing a common trend, such that the overall uncertainty only depends on the sum of lengths of the two series, here 120 months (Figure 4).

[32] To illustrate how to use Figure 4, we simulate the detection of a ω value of 0.01/12 mg m^{-3} month^{-1} within the two time series of 60 months with a ϕ value equal to 0.6 and a σ value equal to 0.03. Considering an overlap of 1 year, the detection value, $|\omega|/\sigma_\omega = |\omega|/(G\sigma) = (0.01/12)/(0.03 \times 0.0095) = 2.19$, i.e., the 95% level of confidence is reached. Conversely, for the 1 year gap situation, $|\omega|/\sigma_\omega = (0.01/12)/(0.05 \times 0.013) = 1.28$, i.e., this trend would not be detected if analyzed with the same number of monthly observations but with disjoint time series.

[33] We also depict the evolution of uncertainty G as a function of the length of the second time series, with a given length of the first time series set to 60 months. We test for two different situations: a 1 year time overlap (Figure 5a) with α value set to 0.7, and a 1 year gap (Figure 5b). In both cases, uncertainty G increases with ϕ and decreases with the length of the second time series. For a 1 year overlap and for a moderately high value of ϕ of 0.6, a typical value observed in Figures 1b and 2b, G values are 0.015 and 0.0125 after a duration of 12 and 36 months for the second time series, respectively, i.e., σ_w has decreased of 16%. For a 1 year gap, for the same value of ϕ, G values are 0.019 and 0.018, respectively, i.e., σ_w has decreased of 5% in 2 years and is 26% greater at 12 months and 44% at 36 months compared to the overlap situation.

[34] The impact of new available space-based observations such as provided by the incoming S3 satellite with onboard the OLCI sensor may also be evaluated using the

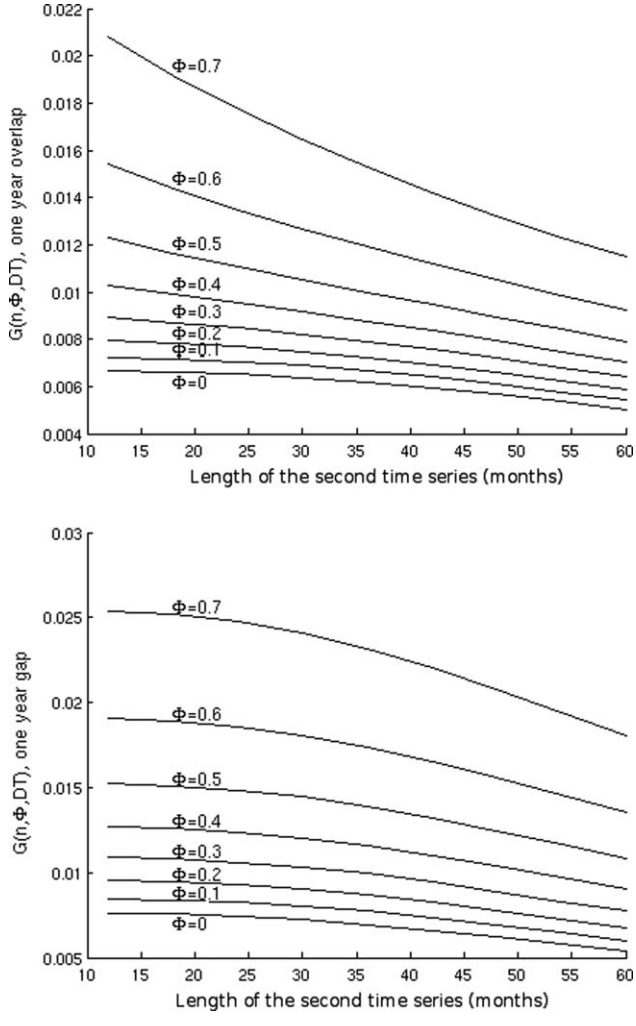

Figure 5. Effect of the length of the second time series on the uncertainty trend coefficient G (equation (9)) with (a) a 1 year overlap and (b) a 1 year gap.

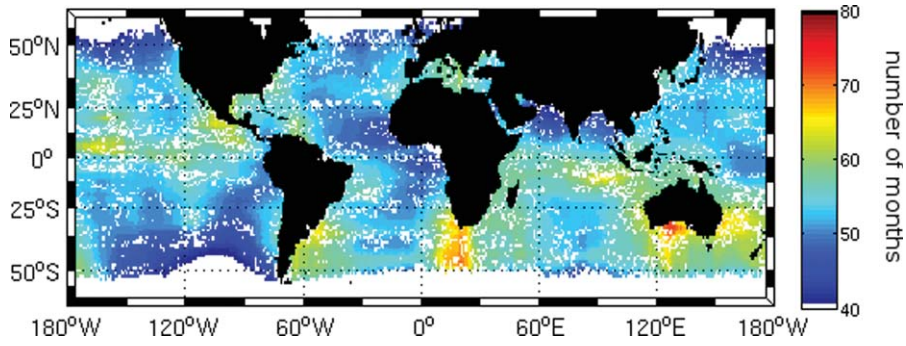

Figure 6. Estimated duration of needed Sentinel 3-OLCI month measurements to enhance the joint SeaWiFS-MERIS detection of long-term linear trend: from simulations of model (equation (9), see text for details).

proposed model (equation (9)). This satellite should be launched at the end of 2014, and consequently, no overlap will be observed with the MERIS, SeaWiFS, and MODIS time series (MODIS-AQUA, launched in 2002, mission's initial lifetime was planned to be about 6 years). To evaluate the added value of the S3 mission regarding the long-term trend detection, we consider here that the uncertainty on the level shift between OLCI and MERIS OC4 derived chl-a will be of the same magnitude than the one estimated between MERIS OC4 and SeaWiFS OC4 (not shown). Given this assumption, we proceed as previously to determine the variance of the trend estimate (Appendix B).

[35] We proceed as follows to derive a global map (Figure 3). For locations such that $|\hat{\omega}|/\sigma_{\hat{\omega}} > 0.5$, i.e., a 70% significance level, we assume that the trend estimate $\hat{\omega}$ might be relevant but was not detected as significant due to a too low number of MERIS-SeaWiFS observations compared to observed local noise level. From simulations, we determine the required duration of the OLCI time series to reach a 95% significance level, i.e., $|\hat{\omega}|/\sigma_{\hat{\omega}} > 1.96$. For locations with significant SeaWiFS-MERIS linear trend estimate with a 95% significance level, we determine from simulations the required duration of the OLCI time series to reduce the uncertainty $\sigma_{\hat{\omega}}$. For these numerical derivations, we also assume in equation (9) that ${\sigma_1}^2 = {\sigma_2}^2$, i.e., the white noise variance measured from OLCI will be equal to the white noise variance estimated from the SeaWiFS-MERIS data set (Figure 3c). The starting time of the OLCI time series is the first January 2015 leading to a T_0 value of 36 months (MERIS time series ends here in December 2011). Overall, the reported results show that a mean duration of 53 months of S3-OLCI observations will be necessary to actually enhance the detection of significant linear trends issued from the joint SeaWiFS-MERIS analysis (Figure 6). Interestingly, results are spatially homogeneous with local variability related to region-specific noise characteristics. In the South Pacific, the west of Senegal, and the Arabian Sea, a minimum of 40 months of S3-OLCI is needed to enhance the detection. In these areas a trend is nearly detected. In the south part of America, South Africa, and the south of Australia, high estimated values of $\hat{\sigma}$ lead to an increase of $\sigma_{\hat{\omega}}$, and a longer duration of S3-OLCI observations (typically about 68 months) will be necessary. In the Equatorial Pacific, the variance of the noise is low, but the significant estimated trends are very weak increasing the time of S3-OLCI observations necessary to actually improve the detection of significant long-term trends.

5. Conclusions

[36] The two major statistical factors governing a trend estimation and detection in a single-sensor time series are the autocorrelation and the variance of the noise. The estimated noise autocorrelation showed latitudinal distribution with a mean value of 0.35 in equatorial zones compared to 0.25 at higher latitudes. This difference leads to an increase of 16% of the uncertainty on the estimation of the same trend in these two different areas. When two time series are available, the trend detection depends also on the uncertainty on the level shift between the data sets. In case of an overlap, the shift uncertainty is diminished. The use of the joint chl-a SeaWiFS-MERIS data set over the period 1998–2011 led to the detection of 60% of significant trends, compared to 41% for the SeaWiFS data set only and 50% for the MERIS data set only, contributing to a better characterization of region-specific patterns in the detected trends.

[37] Optimizing an observation network for the long-term monitoring implies to minimize the effect of the unknown level shift by organizing time overlaps between successive missions. From our analysis and for a noise autocorrelation level greater than 0.3 as observed in average for our data set, an overlap of 12 months has been found to be optimal to lower the uncertainty on the level shift and to minimize the uncertainty on the trend estimate within two time series of 60 months.

[38] In case the time series present no time overlap, the estimation of a potential level shift and its uncertainty is needed. This can be derived from intercalibration analyses based on the physical characteristics of the sensor measurements, as well as from intercalibration based on comparison with consistent long-term field observations [*Antoine et al.*, 2008; *Clark et al.*, 2003]. This aspect, which should be addressed in future works, is crucial for a meaningful merging of the incoming Sentinel 3-OLCI time series with previous ocean-color missions. Savings, in terms of necessary duration of Sentinel 3-OLCI observations and resulting costs, is grandly constrained by this issue. In this respect, we estimated the minimal region-dependent duration of the Sentinel 3-OLCI mission necessary to improve the detection of long-term linear trends issued from the SeaWiFS-MERIS data set.

We estimated a mean value of 53 months for the needed Sentinel 3-OLCI observations, with some region-dependent fluctuations between 40 and 68 months. This simulation was carried out using an uncertainty level on the shift between OLCI and MERIS of the same magnitude than the one estimated between SeaWiFS and MERIS. These results are coherent with the expected lifetime of the Sentinel 3-OLCI mission and suggest that the analysis of the global long-term patterns should actually benefit from the joint analysis of SeaWiFS, MERIS, and Sentinel 3-OLCI data sets.

[39] In the future, the methodology will be applied to other ocean-color variables such as the vertical attenuation of the light [*Morel et al*., 2007; *Saulquin et al*., 2012]. Its application to in situ data might also be considered, for instance, for validation purposes. Given the noise parameters of the considered remotely sensed data, we were able to detect relatively weak trends, typically between ± 0.01 and ± 0.1 mg m^{-3} decade^{-1}. In situ measurements generally involve greater variance levels caused by support effects, i.e., the local variability in the chl-a, caused by fine-scale structures such as filaments which are averaged using the $1^\circ \times 1^\circ$ satellite data [*Saulquin et al*., 2011]. Such local variability in the in situ data, especially at the shore, alters the trend detection. The design of specific in situ setting (e.g., sensor networks) might require to reduce these variances to detect linear trend levels similar to those issued from remotely sensed data. Regarding methodological aspects, refined models of level shift between time series (magnitude-dependent models) and the effect of outliers in the estimation of the autoregressive parameters [*Sarnaglia*, 2010] should also be evaluated. The influence of low-frequency climatic signal such as ENSO on the ocean-color data set should also be considered with care. In this respect, the development of specific filtering procedures to remove such contributions could be investigated.

Appendix A

[40] This appendix details the estimation procedure for shared linear trends in two time series involving autocorrelated noise processes. Formally, we consider the following model:

$$y_t = \mu + \omega t + \delta U + S_t + N_{1t}, + N_{2t} \tag{A1}$$

[41] To correct for the autocorrelation term (equation (8)) the following transformation is applied to resort to uncorrelated variables.

A1. Transformation

[42] For periods where only one time series is present, the standard Cochrane and Orcutt transformation is applied:

$$y_t^* = y_t - \phi y_{t-1}$$

[43] When only the first time series is present, equation (8a) turns into

$$y_{1t}^* = \mu(1-\phi_1) + \omega\phi_2 + \omega(1-\phi_1)t + \epsilon_{1t},$$
$$t = 1 \ldots n_1 \quad \text{and} \quad \epsilon_{1t} \sim N\left(0, {\sigma_1}^2\right)$$

[44] When only the second time series is present, equation (8b) turns into

$$y_{2t}^* = \mu(1-\phi_2) + \omega\phi_2 + \omega(1-\phi_2)t + \quad \delta(1-\phi_2)t + \epsilon_{2t},$$
$$t = T_0 \ldots n_2 \text{ and } \epsilon_{2t} \quad \sim N\left(0, {\sigma_2}^2\right)$$

[45] When both time series are present, we suppose that the white noises are correlated together, and the following transformation is applied:

$$y_t^* = y_{1t} - \phi_1 y_{2t-1}$$

$$y_t^* = \mu(1-\phi_1) + \omega\phi_1 + \omega\phi_2 + \omega(1-\phi_1)t + \epsilon_{3t},$$
$$t = T_0, \ldots, n_1$$

[46] With $\epsilon_3 = \epsilon_1 - \alpha\epsilon_2$

$$\sigma_3^2 = E(\epsilon_3 - E(\epsilon_3))^2 = E(\epsilon_1 - \alpha\,\epsilon_2)^2 = \sigma_1^2 + \alpha^2 \times \sigma_2^2$$

and

$$\alpha = \frac{\sigma_{12}}{\sigma_1 \quad \sigma_2}$$

A2. Model Parameter Estimation

[47] The transformed equation can be expressed using the matrix form:

$$Y^* = X^* A + \epsilon$$

where X^* is either a $T \times 3$ matrix (μ, δ, ω) or a $T \times 11$ matrix when considering a seasonal signal $S(t)$. A is a vector containing the parameters to be estimated and ε is the residual white noise. Hence, the GLS estimator resorts to OLS estimator of A:

$$\hat{A} = \left(X^{*\prime}\gamma^{-1}X\right)^{-1} X^{*\prime}\gamma^{-1}Y^*$$

with γ being the covariance matrix of the residuals ε (the variance of the residuals is time series dependent). The parameter γ is diagonal with values equal to $\hat{\sigma}_1{}^2$, $\hat{\sigma}_2{}^2$, $\hat{\sigma}_3{}^2$ (depending how you order the data). $X^{*\prime}$ stands for the transpose of X^*. In practice, the equation must be solved using an iterative process. First, the values of $\hat{\phi}_1$, $\hat{\phi}_2$, $\hat{\sigma}_1$, $\hat{\sigma}_2$, $\hat{\sigma}_3$, and α must be evaluated from the data. Then $\hat{A}$ is estimated. The values of $\hat{\phi}_1$, $\hat{\phi}_2$, $\hat{\sigma}_1$, $\hat{\sigma}_2$, $\hat{\sigma}_3$, and $\hat{\alpha}$ are then revaluated. The iterative procedure is iterated until convergence. The estimated covariance matrix of $\hat{A}$ is obtained using

$$COV\left(\hat{A}\right) = \left(X^{*\prime}\gamma^{-1}X\right)^{-1}$$

Appendix B

[48] This appendix details the computation of the uncertainty on the model parameter estimate $\hat{A}$. If the uncertainty σ_0 of the level shift is estimated from external sources (independent cross calibration of sensors, theoretical model, etc.), the covariance matrix of the estimate $\hat{A}$ is given by

$$COV\left(\hat{A}\right) = \left(X^{*\prime}\gamma^{-1}X^{*\prime} + \sigma^2\gamma_2\right)^{-1}$$

with

$$\gamma_2 = \begin{bmatrix} 0 & 0 & 0 \\ 0 & 0 & 0 \\ 0 & 0 & \dfrac{1}{\sigma 0} \end{bmatrix}$$

where σ^2 is the weighted average of the noise variance of the two time series:

$$\sigma^2 = \frac{\sum_{t=1}^{T1}(t - t_{median})^2\sigma_1^2 + \sum_{t=T0}^{T}(t - t_{median})^2\sigma_2^2}{\sum_{t=1}^{T1}(t - t_{median})^2 + \sum_{t=T0}^{T}(t - t_{median})^2}$$

with $t_{median} = median(t_1, t_2)$ and σ_1^2 and σ_2^2 being the white noise variances of the two time series.

[49] **Acknowledgments.** This work has been partly supported by the AquaMar project that has received funding from the European Community's Seventh Framework Program FP7/2007–2013 under grant agreement FP7-SPACE-2009-1/collaborative project 241759 FP7.

References

Aitken, C. (1935), On least squares and linear combinations of observations, *Proc. R. Soc. Edinburgh*, *55*, 42–48.

Alexander, M. A., L. Matrosova, C. Penland, J. D. Scott, and P. Chang (2008), Forecasting Pacific SSTs: Linear inverse model predictions of the PDO, *J. Clim.*, *21*, 385–402.

Antoine, D., A. Morel, H. R. Gordon, V. F. Banzon, and R. H. Evans (2005), Bridging ocean color observations of the 1980s and 2000s in search of long-term trends, *J. Geophys. Res.*, *110*, C06009, doi:10.1029/2004JC002620.

Antoine, D., F. D'Ortenzio, S. B. Hooker, G. Bécu, B. Gentili, D. Tailliez, and A. J. Scott (2008), Assessment of uncertainty in the ocean reflectance determined by three satellite ocean color sensors (MERIS, SeaWiFS and MODIS-A) at an offshore site in the Mediterranean Sea (BOUSSOLE project), *J. Geophys. Res.*, *113*, C07013, doi:10.1029/2007JC004472.

Blunden, J., D. S. Arndt, and M. O. Baringer (2011), State of the climate in 2010, *Bull. Am. Meteorol. Soc.*, *92*, S1–S236.

Boyce, D. G., M. R. Lewis, and B. Worm (2010), Global phytoplankton decline over the past century, *Nature*, *466*, 591–596, doi:10.1038/nature09268.

Clark, D. K., M. A. Yarbrough, M. Feinholz, S. Flora, W. Broenkow, Y. S. Kim, B. C. Johnson, S. W. Brown, M. Yuen, and J. L. Mueller (2003), MOBY, a radiometric buoy for performance monitoring and vicarious calibration of satellite ocean color sensors: Measurement and data analysis protocols, in *Ocean Optics Protocols for Satellite Ocean Color Sensor Validation*, vol. *VI*, *NASA Tech. Memo. 2003-211621/Rev4*, edited by J. L. Mueller, G. S. Fargion, and C. R. McClain, p. 43, NASA Goddard Space Flight Cent., Greenbelt, Md.

Clifford, P., S. Richardson, and D. Hemon (1989), Assessing the significance of the correlation between two spatial processes, *Biometrics*, *45*(1), 123–134, doi:10.2307/2532039.

Cochrane, D., and G. H. Orcutt (1949), Application of least squares regression to relationships containing auto-correlated error terms, *J. Am. Stat. Assoc.*, *44*(245), 32–61.

Compo, G. P., and P. D. Sardeshmukh (2010), Removing ENSO-related variations from the climate record, *J. Clim.*, *23*(8), 1957–1978, doi:10.1175/2009JCLI2735.1.

Davidson, R., and J. G. MacKinnon (1993), *Estimation and Inference in Econometrics*, Oxford University Press, New York.

Dutilleul, P. (1993), Modifying the t-test for assessing the correlation between two spatial processes, *Biometrics*, *49*(1), 305–314, doi:10.2307/2532625.

Evans, R. H., and H. R. Gordon (1994), Coastal zone color scanner 'system calibration': A retrospective examination, *J. Geophys. Res.*, *99*, 7293–7307, doi:10.1029/93JC02151.

Frankignoul, C., and K. Hasselmann (1977), Stochastic climate models. Part II: Application to SST anomalies and thermocline variability, *Tellus*, *29*, 289–305.

Gregg, W. W., and N. W. Casey (2004), Global and regional evaluation of the SeaWiFS chlorophyll data set, *Remote Sens. Environ.*, *93*(4), 463–479.

Gregg, W. W., N. W. Casey, and C. R. McClain (2005), Recent trends in global ocean chlorophyll, *Geophys. Res. Lett.*, *32*, L03606, doi:10.1029/2004GL021808.

Haan, C. T. (1977) *Statistical Methods in Hydrology*, 378 pp., Iowa State Univ. Press, Ames.

Henson, S. A., J. L. Sarmiento, J. P. Dunne, L. Bopp, I. Lima, S. C. Doney, J. John, and C. Beaulieu (2010), Detection of anthropogenic climate change in satellite records of ocean chlorophyll and productivity, *Biogeosciences*, *7*, 621–640, doi:10.5194/bg-7-621-201.

Hooker, S. B., W. E. Esaias, G. C. Feldman, W. W. Gregg, and C. R. Mc Clain (1992), An overview of SeaWiFS and ocean color, in *SeaWiFS Technical Report Series*, NASA Tech. Memo. 104566, edited by S. B. Hooker and E. R. Firestone, pp. 9–25, NASA Goddard Space Flight Cent., Greenbelt, Md.

International Ocean-Color Coordinating Group (2000), *Remote Sensing of Ocean Colour in Coastal, and Other Optically-Complex, Waters*, edited by S. Sathyendranath, p. 140, Reports of the International Ocean-Colour Coordinating Group, No. 3, IOCCG, Dartmouth, Canada.

International Ocean-Color Coordinating Group (2010), *Atmospheric Correction for Remotely-Sensed Ocean-Color Products*, edited by M. Wang, Rep. of the Int. Ocean-Color Coord. Group 10, Dartmouth, Canada.

Johnson, B. C., S. S. Bruce, E. A. Early., J. M. Houston, T. R. O'Brian, A. Thompson, S. B. Hooker, and J. L. Mueller (1996), *The Fourth SeaWViFS Intercalibration Round-Robin Experiment (SIRREX-4)*, in *SeaWiFS Technical Report Series*, vol. *37*, NASA Goddard Space Flight Cent., Greenbelt, Md.

Legendre, P., and L. Legendre (1998), *Numerical Ecology*, 3rd English ed., xv + 853 pp., Elsevier, Amsterdam.

Maritorena, S., O. Hembise Fanton d'Andon, A. Mangin, and D. A. Siegel (2010), Merged satellite ocean color data products using a bio-optical model: Characteristics, benefits and issues, *Remote Sens. Environ.*, *114*(8), 1791–1804, doi:10.1016/j.rse.2010.04.002.

McClain, C. R. (2009), A decade of satellite ocean color observations, *Annu. Rev. Mar. Sci. 1*(1), 19–42.

Morel, A., B. Gentili, M. Chami, and J. Ras (2006), Bio-optical properties of high chlorophyll Case 1 waters, and of yellow substance-dominated Case 2 waters, *Deep Sea Res.*, *53*, 1439–1459.

Morel, A., Y. Huot, B. Gentili, P. J. Werdell, S. B. Hooker, and B. A. Franz (2007), Examining the consistency of products derived from various ocean color sensors in open ocean (Case 1) waters in the perspective of a multi-sensor approach, *Remote Sens. Environ.*, *111*, 69–88.

O'Reilly, J. E., S. Maritorena, B. G. Mitchell, D. A. Siegel, K. L. Carder, S. A. Garver, M. Kahru, C. McClain (1998), Ocean color algorithms for SeaWiFS, *J. Geophys. Res.*, *103*, 24,937−24,953, doi:10.1029/98JC02160.

O'Reilly, J. E., et al. (2000), Ocean color chlorophyll-a algorithms for SeaWiFS, OC2, and OC4: Version 4, in *SeaWiFS Postlaunch Calibrationnd Validation Analyses, Part 3*, vol. 11, edited by S. B. Hooker and E. R. Firestone, pp. 9–23, NASA, Goddard Space Flight Center, Greenbelt, Md.

Pezzulli, S., D. B. Stephenson, and A. Hannachi (2005), The variability of seasonality, *J. Clim.*, *18*, 71−88, doi:10.1175/JCLI-3256.1.

Philander, S. G. (1990), El Niño, La Niña, and the Southern Oscillation, *Int. Geophys.*, *46*..

Philander, S. G. (1990), El Niño, La Niña, and the Southern Oscillation, *Int. Geophys.*, *46*..

Polovina, J. J., E. A. Howell, and M. Abecassis (2008), Ocean's least productive waters are expanding, *Geophys. Res. Lett.*, *35*, L03618, doi:10.1029/2007GL031745.

Prais, S. J., and C. B. Winsten (1954), Trend estimators and serial correlation, *Discus. Pap. 383*, Cowles Comm., Chicago, Ill.

Rast, M., J. L. Bézy, and S. Bruzzi (1999), The ESA Medium Resolution Imaging Spectrometer MERIS—A review of the instrument and its mission, *Int. J. Remote Sens.*, *20*, 1681–1702.

Salomonson, V. V., D. L. Toll, and W. T. Lawrence (1992), The moderate resolution imaging spectrometer (MODIS) and observations of the land surface, in *Proceedings of the IGARSS 92 Symposium*, 26−29 May, pp. 549−551, Institute of Electrical and Electronics Engineers, Inc., N. Y.

Sarnaglia, A. J. (2010), Estimation of periodic autoregressive processes in the presence of additive outliers, *J. Multivariate Anal. Arch.*, *101*(9), 2168–2183.

Saulquin, B., F. Gohin, and G. Rene (2011), Regional objective analysis for merging high-resolution MERIS, MODIS/Aqua, and SeaWiFS chlorophyll-a data from 1998 to 2008 on the European Atlantic Shelf, *IEEE Trans. Geosci. Remote Sens.*, *49*(1), 143–154.

Saulquin, B., A. Hamdi, F. Gohin, and J. Populus (2012), Estimation of the diffuse attenuation coefficient KdPAR using MERIS and application to seabed habitat mapping, *Remote Sens. Environ.*, *128*, 224–233, doi:10.1016/j.rse.2012.10.002.

Scherrer, B. (1984), *Biostatistique*, xix + 850 pp., Gaëtan Morin Ed., Boucherville, France.

Tiao, G. C., G. C. Reinsel, D. Xu, J. H. Pedrick, X. Zhu, A. J. Miller, J. J. DeLuisi, C. L. Mateer, and D. J. Wuebbles (1990), Effects of autocorrelation and temporal sampling schemes on estimates of trend and spatial correlation, *J. Geophys. Res.*, *95*(D12), 20,507–20,517, doi:10.1029/JD095iD12p20507.

Torrence, C., and P. J. Webster (1998), The annual cycle of persistence in the El Niño–Southern Oscillation, *Q. J. R. Meteorol. Soc.*, *124*, 1985–2004.

Turk, D., C. S. Meinen, D. Antoine, M. J. McPhaden, and M. R. Lewis (2011), Implications of changing El Niño patterns for biological dynamics in the equatorial Pacific Ocean, *Geophys. Res. Lett.*, *38*, L23603, doi:10.1029/2011GL049674.

Vantrepotte, V., and F. Mélin (2009), Temporal variability of 10-year global SeaWiFS time-series of phytoplankton chlorophyll a concentration, *ICES J. Mar. Sci.*, *66*, 1547–1556.

Weatherhead, E. C., et al. (1998), Factors affecting the detection of trends: Statistical considerations and applications to environmental data, *J. Geophys. Res.*, *103*(D14), 17,149–17,161, doi:10.1029/98JD00995.